Article

Hybrid AC/DC Microgrid Energy Management Strategy Based on Two-Step ANN

Tae-Gyu Kim [ID], Hoon Lee [ID], Chang-Gyun An, Junsin Yi and Chung-Yuen Won *

Department of Electrical and Computer Engineering, Sungkyunkwan University, Suwon 16419, Republic of Korea
* Correspondence: woncy550@gmail.com; Tel.: +82-31-290-7169

Abstract: In grid-connected operations, a microgrid can solve the problem of surplus power through regeneration; however, in the case of standalone operations, the only method to solve the surplus power problem is charging the energy storage system (ESS). However, because there is a limit to the capacity that can be charged in an ESS, a separate energy management strategy (EMS) is required for stable microgrid operation. This paper proposes an EMS for a hybrid AC/DC microgrid based on an artificial neural network (ANN). The ANN is composed of a two-step process that operates the microgrid by outputting the operation mode and charging and discharging the ESS. The microgrid consists of an interlinking converter to link with the AC distributed system, a photovoltaic converter, a wind turbine converter, and an ESS. The control method of each converter was determined according to the mode selection of the ANN. The proposed ANN-based EMS was verified using a laboratory-scale hybrid AC/DC microgrid. The experimental results reveal that the microgrid operation performed stably through control of individual converters via mode selection and reference to ESS power, which is the result of ANN integration.

Keywords: energy management strategy; distributed generation; interlinking converter; artificial neural network; hybrid AC/DC microgrid

1. Introduction

Recently, the power generated by renewable energy sources, such as solar power and wind power generation, has increased. However, there are several variables that affect centralized power supply methods. Because of these challenges, interest in microgrids that perform local generation and consumption of power by arranging distributed generation (DG) centered on customers is increasing. Research on methods and operations for linking AC-based centralized power supply systems with DC microgrids is underway [1–3].

Figure 1 illustrates microgrid configurations according to voltage type. Figure 1a shows the AC microgrid. The AC microgrid has the advantage of being able to supply power in connection with the AC distributed system [4]; therefore, the initial installation cost is low, and the existing load can be used as the distribution system voltage is in the form of AC. However, when large-scale DG is a factor, the microgrid's stability and power factor are adversely affected, and power generation sources, such as solar and wind power, must undergo a two-step power conversion process, resulting in low efficiency. Figure 1b shows a DC microgrid. Unlike an AC distributed system, the DC microgrid does not need to consider reactive power, power factor, or frequency. In addition, the power conversion step of the linked DG source is reduced, and power generation efficiency is increased [5,6]. However, because existing loads are based on AC voltage, there is a disadvantage in that additional power conversion facilities are required.

Because microgrids have distinctive strengths and weaknesses according to voltage, research on hybrid AC/DC microgrids that can connect DC microgrids and AC distributed systems is underway. Figure 1c shows the hybrid microgrid. The hybrid microgrid can be

operated in connection with an AC distributed system (grid-connected) and independently in islands and mountains (standalone) [7–9].
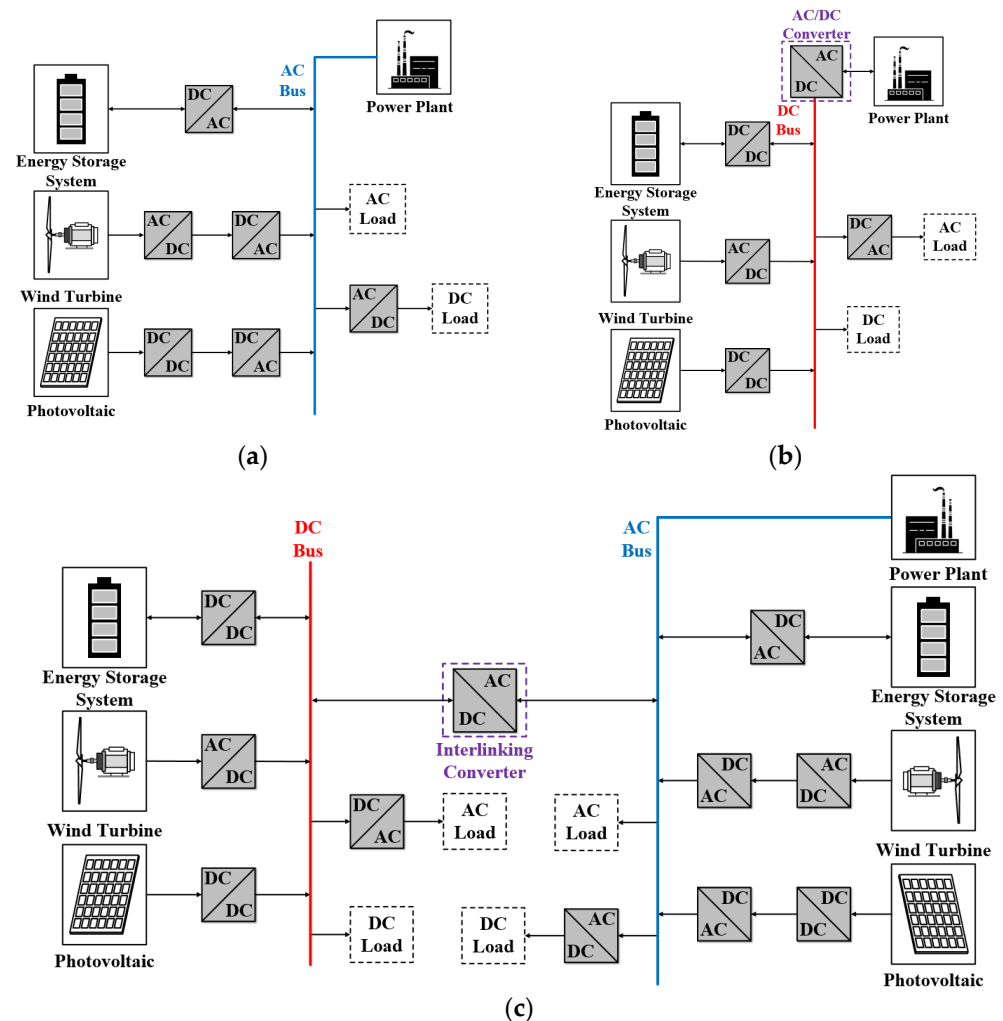

Figure 1. Classification of microgrids with voltage type (**a**) AC; (**b**) DC; (**c**) hybrid AC/DC.

The hybrid microgrid can have several advantages, such as easy connection with the AC distributed system and increased efficiency of the DG source. To construct a hybrid microgrid, various studies have been conducted on an interlinking converter (ILC) with a bidirectional AC/DC converter to link AC distributed systems and DC microgrids [10,11]. ILC not only has the function of linking AC distributed systems and DC microgrids, but it can also supply energy from AC distributed systems when DC microgrid power is insufficient. In addition, it can supply reactive power when the voltage of AC drops, and it can supply power to a point where an accident has not occurred even when a single-line ground fault occurs [12].

A microgrid uses AC power or renewable solar and wind energy sources as its power source, and an energy storage system (ESS) is required to efficiently use the intermittent energy characteristics of these renewable power sources [13]. An energy management strategy (EMS) is needed for the operation of a microgrid. In grid-connected operation, it can receive surplus power and boost insufficient power. However, in standalone operation, surplus power and insufficient power must be resolved by charging and discharging the ESS and balancing load power and generated power. Even in grid-connected operation, an EMS is required to minimize the power reception from the AC distributed system.

Figure 2 depicts two methods of microgrid operation: the decentralized system and the centralized system. Figure 2a shows a decentralized system that facilitates microgrid

expansion. This control method has the disadvantage that a circulating current flows because voltage control is performed for each converter. When the droop method is applied to suppress such a circulating current, the voltage becomes unstable because the voltage drop, according to the droop coefficient, is different, and the state of other converters is unknown [14–16].
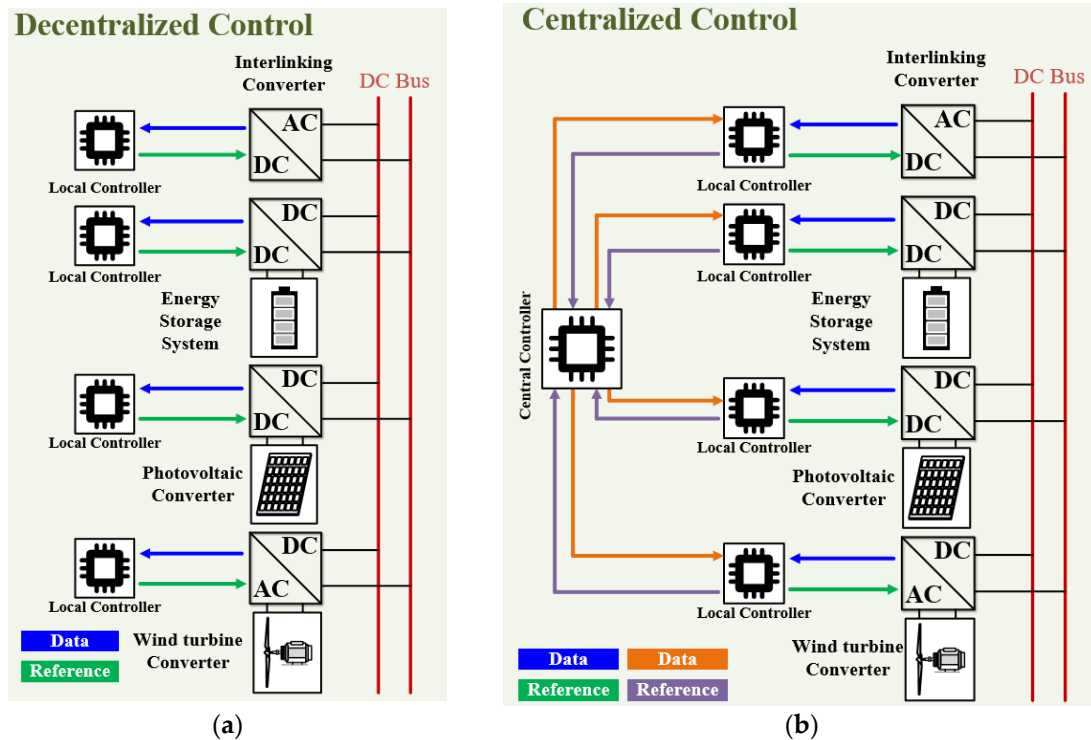

Figure 2. Microgrid control methods: (**a**) distributed system; (**b**) centralized system.

Figure 2b illustrates the centralized system. The centralized system uses a communication line between each converter to monitor power easily. It has the advantage of easy energy management by giving power commands to the ESS based on these monitoring data [17–19]. However, because the method relies heavily on communication, it is vulnerable to communication delay, noise, and accidents.

In this study, the proposed EMS was experimentally verified by applying a centralized control method with the aforementioned advantages.

In the case of conventional EMS, there are several operation modes. Algorithms become complex when considering various situations [20], and the criteria for mode switching are unclear [21].

Because the load pattern of a small-scale regional microgrid does not have a large and constant load pattern, such as that of a building, it is difficult to apply a conventional EMS that predicts load demand [22–24].

For the foregoing reasons, research on microgrid prediction has been conducted, and as part of it, research on artificial intelligence-powered EMS exists [25]. However, it is difficult to apply due to the complexity of the structure and techniques used.

In the conventional EMS mentioned previously, an operation mode is selected with an algorithm. In order to determine the mode with the algorithm, a lot of information is required; the problem is that communication delay is long due to this, and more data must be received from a number of converters. Because of these problems, this paper proposes an EMS that minimizes the information received from the converter using ANN.

Therefore, the proposed method in this paper is summarized as follows.

1. A hybrid microgrid EMS with a two-step process based on an artificial neural network (ANN) is proposed to simplify the operation mode of the conventional complex microgrid and increase the efficiency of ESS power management.

2. The proposed microgrid operation method is applied to the ANN with a two-step structure that reduces the burden of learning compared to a multilayer ANN with only one hidden layer, and it enables easy structural changes by learning individual steps [26].

3. The proposed EMS can easily derive the correct operation mode and ESS power commands based on DG power and load power, which is unpredictable in a small-scale microgrid.

The proposed microgrid EMS was established in a laboratory-scale microgrid to experimentally verify its feasibility.

2. Structure and Operation of Proposed Energy Management Strategy

Figure 3 illustrates the configuration of a hybrid microgrid. The hybrid microgrid can use both AC and DC voltages and has the advantage of being suitable for areas with many islands and mountainous areas. An ILC connects the AC distributed system and DC microgrid, and the ILC is a bidirectional, three-phase, four-leg AC/DC converter, which can maintain the balance of voltages with unbalanced load conditions in the AC distribution system [27].
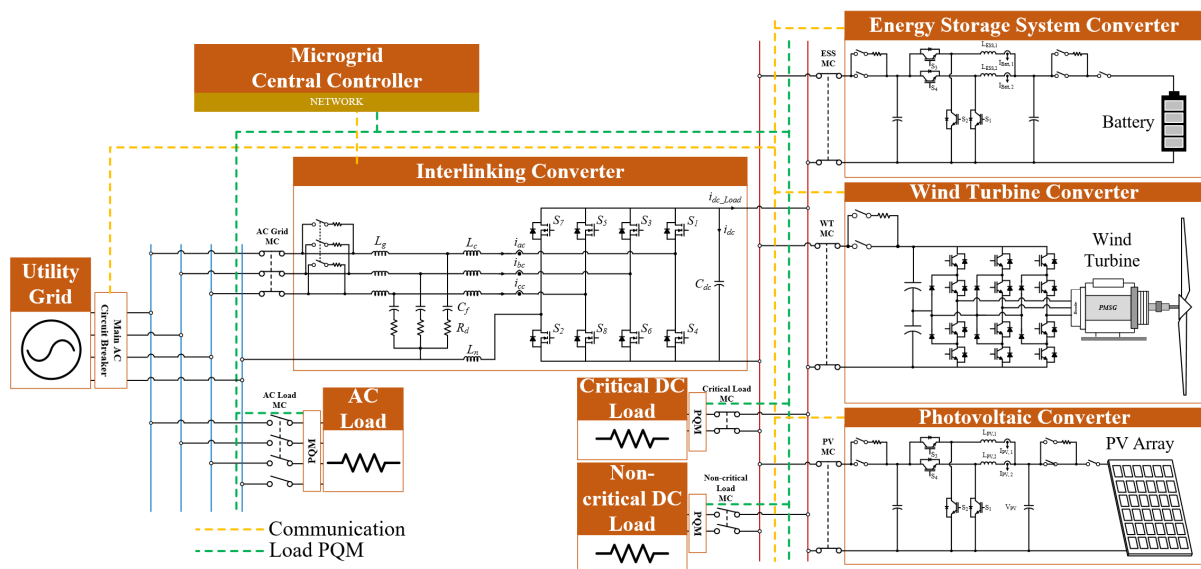

Figure 3. Microgrid configuration with DGs and loads.

2.1. Artificial Neural Network Configuration and Microgrid Control

A DC microgrid is composed of photovoltaic (PV) generators, wind power generators, and an ESS. In standalone operation, it must supply the power to the DC and AC side loads.

In addition, each PV, wind turbine (WT), ESS converter, and load performs power quality monitoring (PQM) through a communication line with a microgrid central controller (MGCC), and the ESS is charged and discharged according to the instructions received from the MGCC. Figure 4a shows the structure of the two-step ANN. The microgrid is operated depending on the first step's output, and the ESS power reference is determined by the output of the second step. Figure 4b shows the structure of the entire converter control block diagram, which is determined by the first step's output.
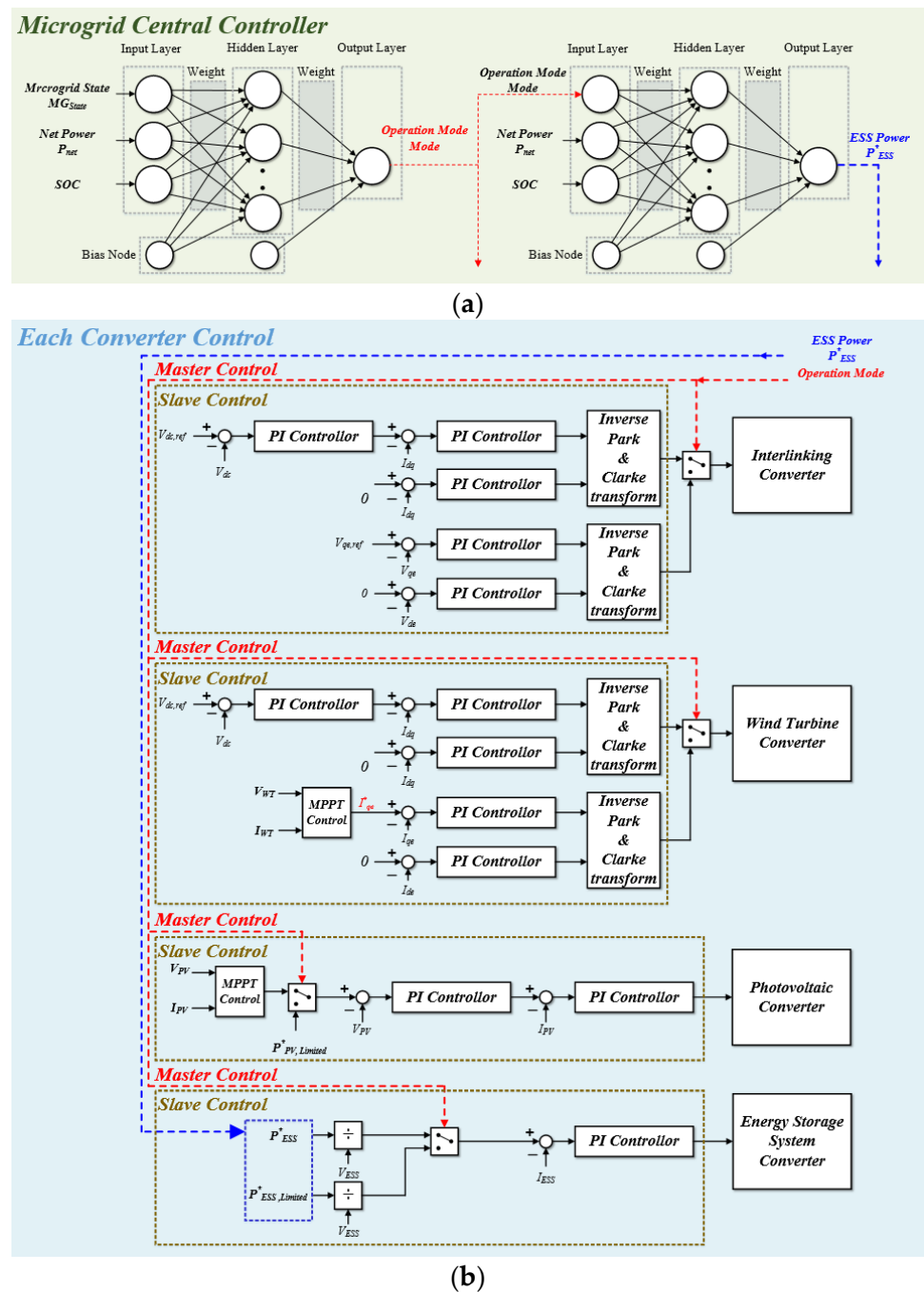
(**a**)

(**b**)

Figure 4. Microgrid control configuration based on ANN. (**a**) Structure of MGCC with proposed two-step ANN for EMS. (**b**) Structure of whole converter control block diagram.

2.1.1. First Step of Artificial Neural Network Operation

The first step has 3 input nodes, 20 hidden nodes, 1 bias node, and 1 output node. Each of the three input nodes consists of MG_{STATE}, microgrid power status, and the state of charge (SOC) of the battery. The output indicates the operating mode of the microgrid. Figure 5 depicts the structure of the ANN. The learned operation mode algorithm is shown in Figure 6. The output of the first step of the ANN is a value between 1 and 5 according to the learned algorithm, and it is composed of the input elements of the second step of the ANN.
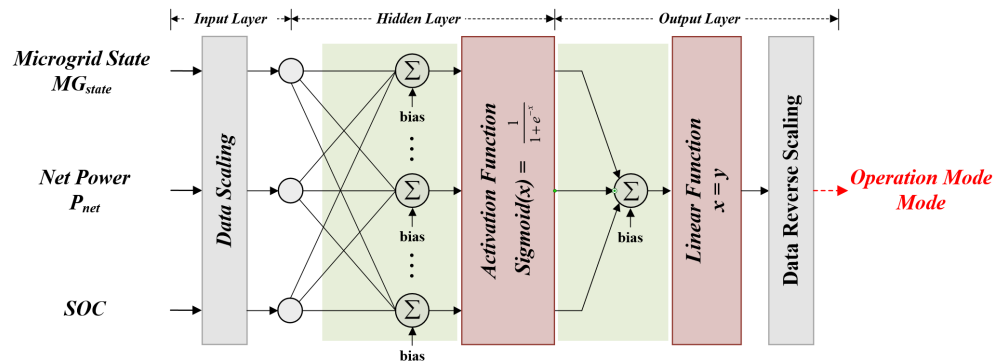
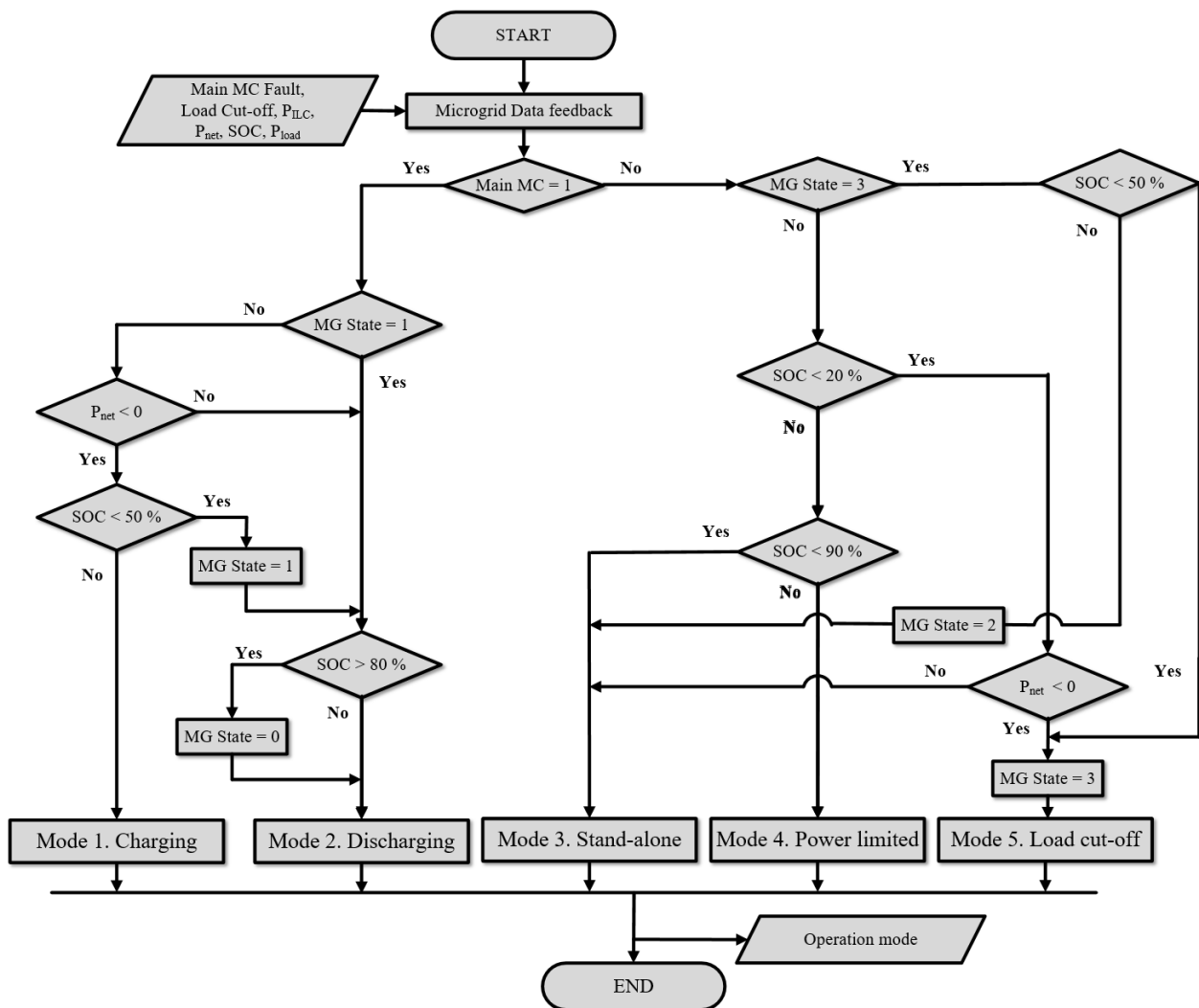**Figure 5.** Configuration of first step of ANN structure.

Figure 6. Operation algorithm of hybrid AC/DC microgrid.

Figure 7 shows the ANN mean square error (MSE). Here, the first step of the ANN process performed 43 iterations for learning, and it was confirmed that the algorithm had an MSE of 3.3642×10^{-6}.
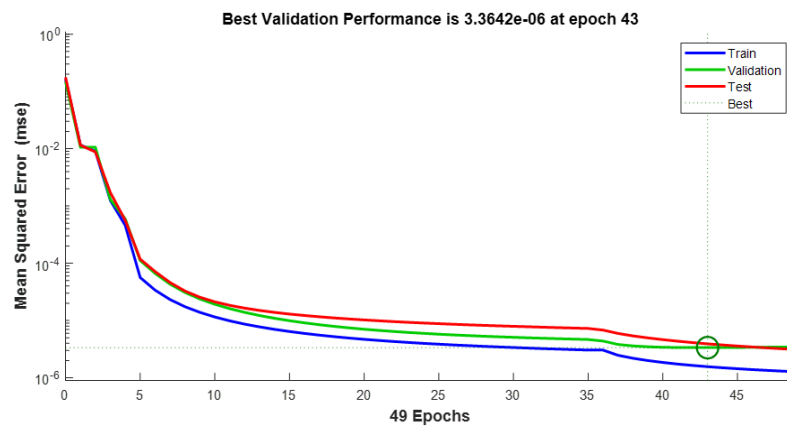
Figure 7. MSE of first step of ANN.

2.1.2. Second Step of Artificial Neural Network Operation

The second step of the ANN's process comprises 3 input nodes, 20 hidden nodes, 1 bias node, and 1 output node. Each of the three input nodes is composed of the *Mode*, which is determined by the first step's output, the power status of the microgrid, and the battery SOC. The output indicates the ESS power command of the microgrid, which is output as a value between −5 kW and 5 kW depending on the input value. Figure 8 illustrates the structure of the second step of the ANN's process.
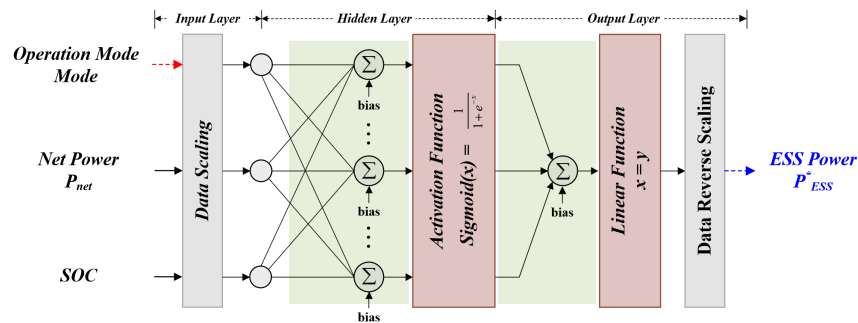

Figure 8. Configuration of second step of ANN structure.

Figure 9 shows the MSE of the ANN. The second step of the ANN's operation performed 48 iterative learning epochs, and it was confirmed that the ESS power command was learned with a mean square error of 1.5837×10^{-5}.
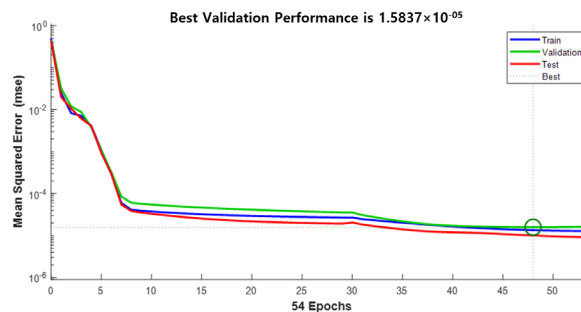

Figure 9. MSE of second step ANN.

2.2. Operation Mode Analysis of AC/DC Hybrid Microgrid Energy Management Strategy

In this paper, we propose a small-scale hybrid microgrid EMS in which a two-step ANN is applied. The MGCC is composed of a two-step ANN: the first step derives the microgrid control mode, and the second step determines the ESS power command for

operation. First, the ILC is essential for connecting the AC distributed system and the DC microgrid. Second, each converter control method is divided into standalone and grid-connected depending on whether they are linked.

In the grid-connected mode, the voltage of the DC microgrid and current of the AC distributed system are controlled by the ILC. The PV and WT converters perform maximum power point tracking (MPPT) control. The ESS operates according to the MGCC's commands. This determines charging and discharging power. In the standalone operation mode, the AC distributed system voltage is controlled by the ILC. The voltage of DC microgrid is controlled by the WT converter. In this mode, the PV converter operates under power-limit and MPPT controls. Detailed operating modes are given in Sections 2.2.1–2.2.4

The microgrid state is divided into four categories, where 0 and 1 correspond to the grid-connected mode, and 2, 3 correspond to the standalone mode. The linkage of the AC distributed system is determined by faults in the main AC circuit breaker in Figure 3. In the case of grid-connected microgrids, the ILC receives approximately 400 W from the grid to maintain DC voltage. With a margin of 2.5 times the minimum amount of power received, it is assumed that if it is less than 1 kW, then power can be supplied from within the microgrid. The power received is expressed as P_{ILC}, and MG_{STATE} is 0. During the grid-connected mode, the ESS SOC must be maintained at 50% or more in preparation for the transition to the independent operation mode. If the SOC of the ESS is less than 50%, then it receives power from the AC distributed system until the SOC becomes 80%, the ESS is charged, and the DC load has received power. The reason for separating MG_{STATE} as described above is to maximize the economic advantages of these microgrids by minimizing the power reception from the AC distributed system.

If a fault occurs in an AC distributed system and the connection to DC microgrid is lost, then the microgrid operates independently. Because power cannot be received or regenerated, like in the grid-connected mode, it is necessary to check the microgrid's power status at all times. When the demand for load is greater than that of the microgrid's distributed power source, the SOC of the ESS will fall below 20% and power cannot be supplied; thus, either a drop in the power distribution network voltage of the microgrid or overdischarge of the ESS occurs. In such a situation, if the cut-off and linkage criteria for non-critical loads are not clearly defined, then the cut-off and linkage are infinitely repeated depending on the SOC of the ESS. Therefore, MG_{STATE} was divided into 2 and 3 even for the standalone mode. When MG_{STATE} is 2, it indicates a load-linked situation, and when MG_{STATE} is 3, it means that the load is a cut-off situation. Table 1 lists the operating mode conditions of each operation.

Table 1. State values of microgrid.

MG_{STATE}		AC Distributed System	P_{ILC}	Load
0	Grid-Connected	0 (on)	<1 kW	-
1		0 (on)	>1 kW	-
2	Standalone	1 (off)	-	Off
3		1 (off)	-	On

2.2.1. Modes 1 and 2: Discharging and Charging Operation

The ILC maintains the DC microgrid's voltage and the AC distributed system's current during grid-connected operation. The ESS is operated according to the MGCC's commands, and each DG source performs MPPT control.

Grid-connected operation is classified into two modes. In the first mode, it does not receive power from the AC distributed system (MG_{STATE} is 0). In the second mode, it receives power from the AC distributed system (MG_{STATE} is 1). When the SOC is sufficient, the operation is performed depending on the command received from the MGCC. If the microgrid has enough power, then there is no reason to receive power from the AC distributed system; therefore, MG_{STATE} is changed to 0. If the SOC is smaller than 50%,

then the ESS will stop discharging and conduct the charging operation until the SOC is over 80%, at which point MG_{STATE} will be changed to 1. Because the power of the microgrid is not enough, it needs to receive power from AC distributed system. Figures 10 and 11 illustrate the flow of the DGs, each converter power during grid-connected operation.
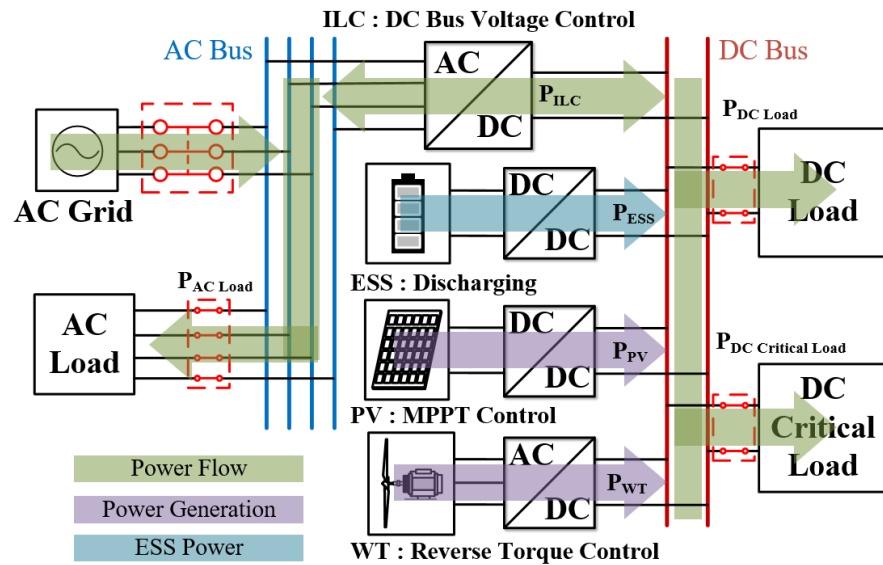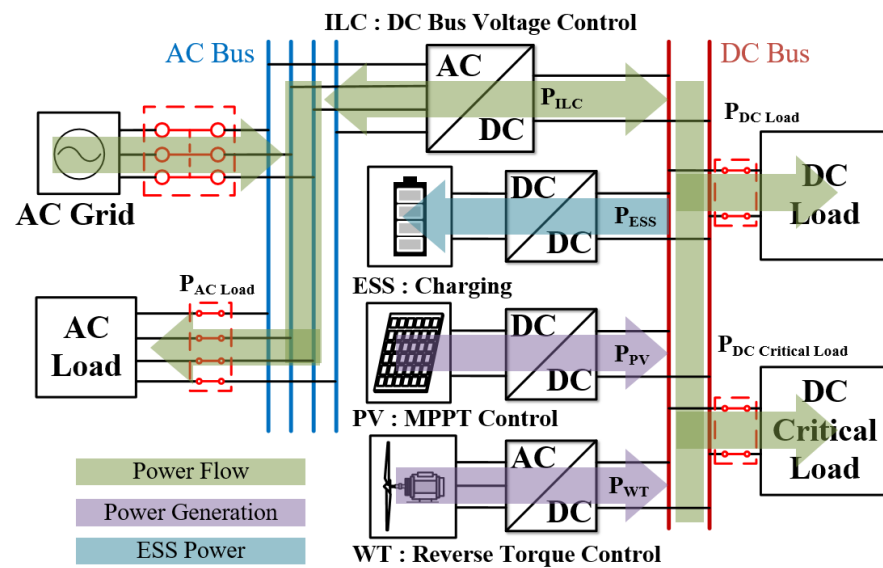

Figure 10. Mode 1: ESS Discharging.

Figure 11. Mode 2: ESS Charging.

2.2.2. Mode 3: Standalone Operation

During standalone operation, the main AC distributed system circuit breaker is turned off. The ILC maintains the AC distributed system's voltage. The WT converter maintains the DC microgrid's voltage.

When the SOC is between 20 and 90%, the mode of microgrid is 3. In mode 3, the ESS conducts charge and discharge operations according to the MGCC's commands. Figure 12 illustrates the flow of the DGs to each converter during standalone operation.
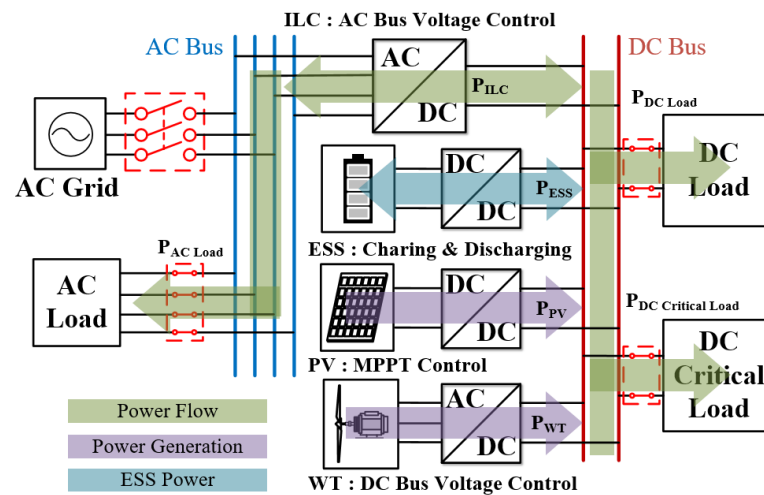
Figure 12. Mode 3: Standalone operation.

2.2.3. Mode 4: Power Limit Operation

Mode 4, power generation limit mode, is included in standalone operation. When the SOC is over 90%, or when there is surplus power even though the ESS cannot be charged anymore because of the high generated power of the distributed power generation source, the mode of microgrid is 4. Mode 4 limits the power of the DGs up to the load power. This mode prevents overcharging and increases the voltage of the DC microgrid. Figure 13 illustrates the flow of power through the DGs and each converter during power limit operation.
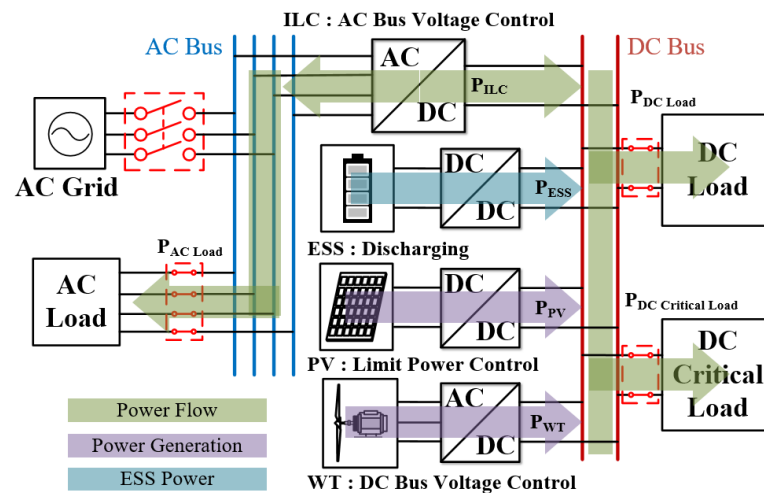

Figure 13. Mode 4: Power Limited Operation.

2.2.4. Mode 5: Cut-Off Load Operation

Mode 5, cut-off load mode, performs an operation to cut off the load.

During standalone operation, in a scenario where the SOC is less than 20% and generation is lower than load demand, the mode of microgrid becomes 5. Because the grid cannot supply power to the load, the load must be cut off.

In mode 5, all DC and AC loads, excluding critical loads, are shed from the microgrid. The ESS conducts its charging operation first. The load is cut off until MG_{STATE} becomes 2. MG_{STATE} changes to 3 when the load is cut off and returns to 2 when the ESS is charged to 50%. At the end of mode 5, non-critical loads are linked back to the microgrid. This mode prevents overdischarging and voltage drops in the DC microgrid. Figure 14 illustrates the flow of power to the DGs and to each converter during cut-off load operation.
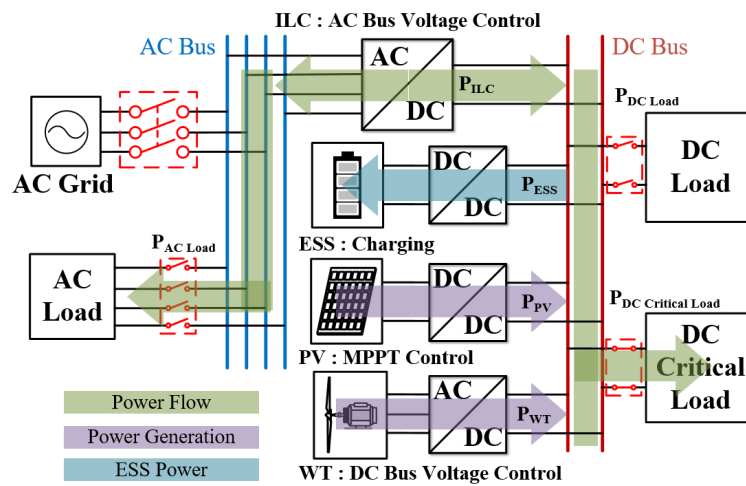
Figure 14. Mode 5: Cut-off load operation.

3. Experiment Results

The experimental equipment were configured as shown in Figure 15 to verify the proposed hybrid microgrid. The individual converters constituting the microgrid are shown in Figures 16–19. The experiment was conducted by simulating the power flow for each mode through the DC and AC loads, and the proposed operation method was verified experimentally.
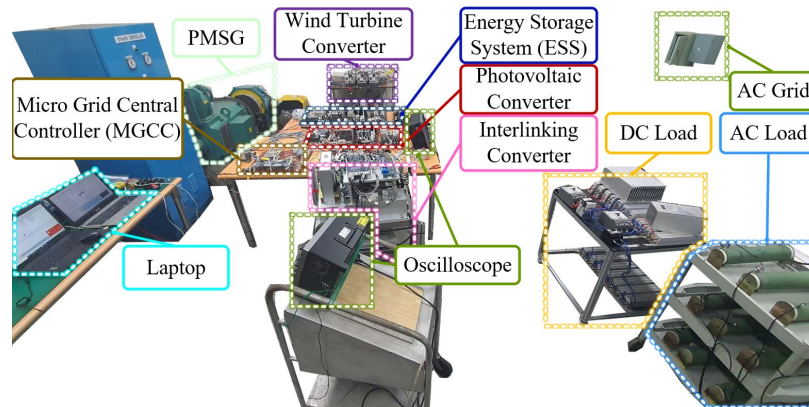

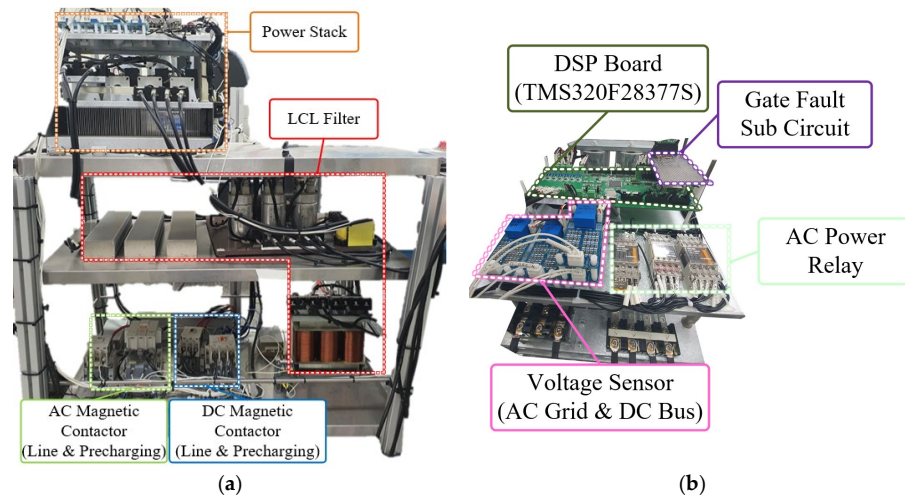**Figure 15.** Small scale microgrid experimental equipment.
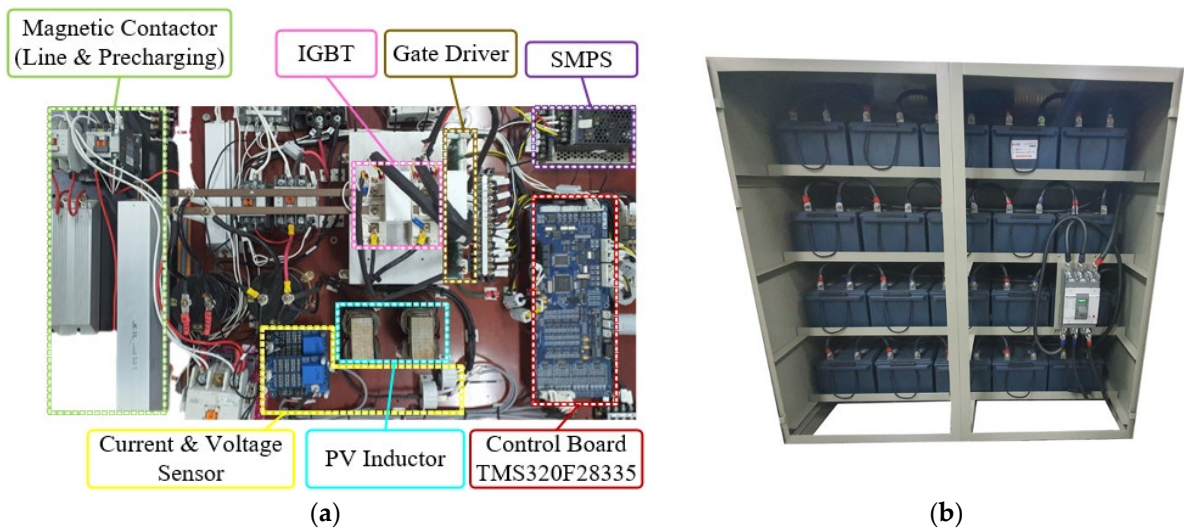

Figure 16. (**a**) ILC; (**b**) power stack of ILC.

Figure 17. Energy storage system (ESS): (**a**) ESS converter; (**b**) battery for ESS.
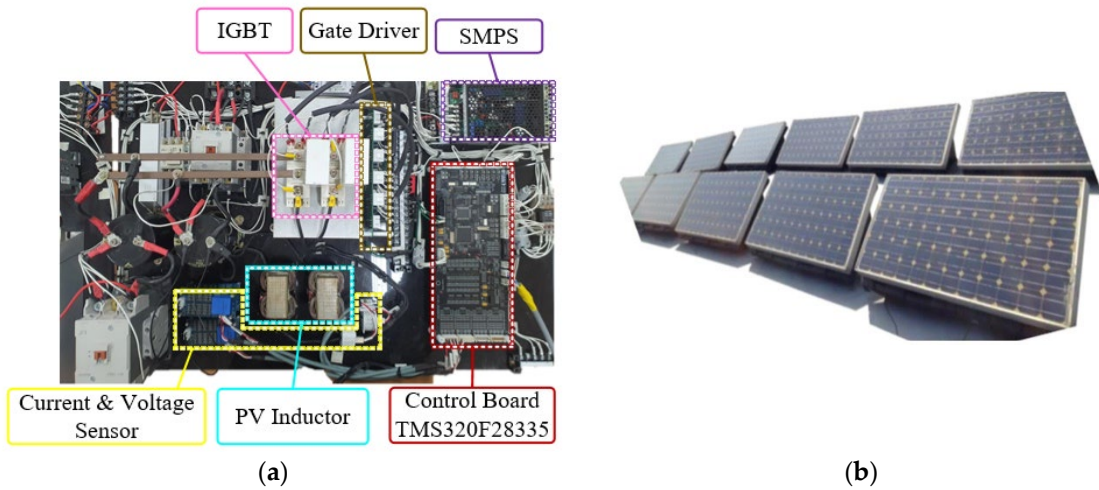

Figure 18. Photovoltaic (PV) generation system: (**a**) PV converter; (**b**) PV panels.
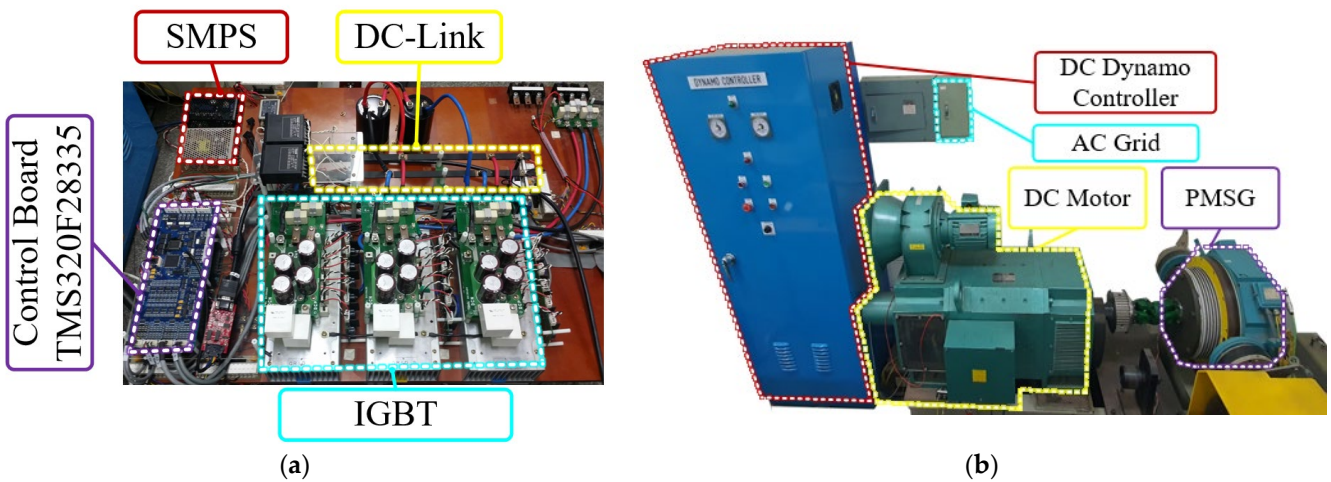

Figure 19. Wind Turbine (WT) generation system: (**a**) 3-level NPC converter; (**b**) M-G set.

Figure 16a,b illustrates the experimental equipment of the ILC and the power stack of the ILC. The topology of the ILC comprises three-phase four-leg converters. When the

AC distributed system is linked, it operates as an AC/DC PWM converter, and in the independent mode, it operates as an inverter.

Figure 17 depicts the configuration of the ESS converter and battery. Each battery had 12 V, and 20 of them were connected in series for a total of 240 V.

Figure 18 illustrates the composition of the PV system and PV panel. A 5 kW class PV panel was used.

Figure 19 shows the WT converter. The WT converter had a DC motor and PMSG connected in series, and it had a capacity of 13.3 kW.

3.1. Experimental Results in Grid-Connected Operation

An experiment was conducted to simulate the case in which the AC distributed system is linked to the microgrid, as shown in Figure 3. In the grid-connected mode, the ILC maintained DC voltage, and the WT and PV converters performed MPPT control.

Figure 20 illustrates the experimental results of the microgrid operating in conjunction with the individual converters through the MGCC. When the SOC was over 50%, the microgrid operation mode was determined according to the output of the first step of the ANN's process, and the charge/discharge power command of the ESS was determined according to the output of the ANN's second step. Section $t_1 \sim t_2$ operated in Mode 1, section $t_2 \sim t_3$ operated in Mode 2, and after t_3, it reverted to Mode 1. Figure 20a illustrates the waveforms of the ANN as the output of MG_{STATE}, SOC, *Mode*, and *ESS Power Reference* as the inputs. Figure 20b illustrates the waveforms of the DC voltage of the microgrid, the output current of the DG converter, the DC load, and the ESS current. Table 2 lists the flow of each converter's power in Modes 1 and 2.
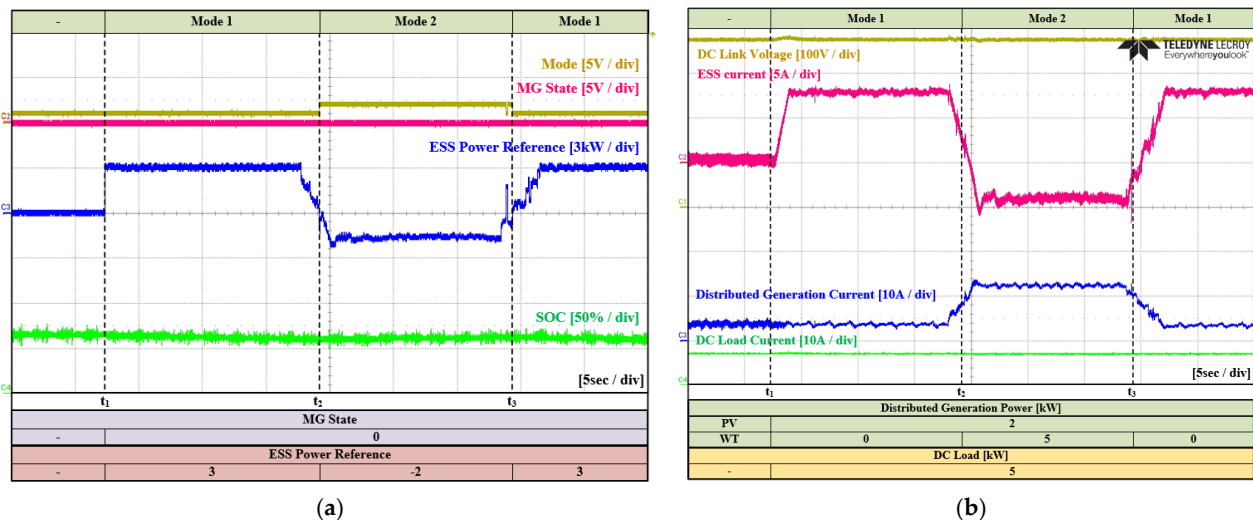

(**a**)   (**b**)

Figure 20. Experimental waveforms of microgrid operation in Modes 1 and 2 during grid-connected operation (1): (**a**) waveforms of input data (MG_{STATE}, SOC) and output data (Mode, ESS power reference) of ANN; (**b**) waveforms of DC link voltage, current of ESS, DG, and DC load.

Table 2. Microgrid power flow (1) in grid-connected operation.

Parameter	Value			Unit
	$t_1 - t_2$	$t_2 - t_3$	After t_3	
Mode	1	2	1	-
ESS	3	−2	3	kW
PV	2	2	2	kW
WT	0	5	0	kW
DC Load	5	5	5	kW

The ANN was input at time t_1; the situation in section t_1–t_2 was given by Equation (1), that of section t_2–t_3 was given by Equation (2), and the mode of ESS operation was selected by the ANN output. In the section after t_3, the same operation as in section t_1–t_2 M

$$P_{Load} > P_{DG} \tag{1}$$

$$P_{Load} < P_{DG} \tag{2}$$

Figure 21 illustrates the experimental waveform in which the SOC of the ESS became 50% or less at time t_4, at which time the ESS was forcibly charged by receiving power from the grid despite the presence of a DC load. Here, the MG_{STATE} was changed to one.
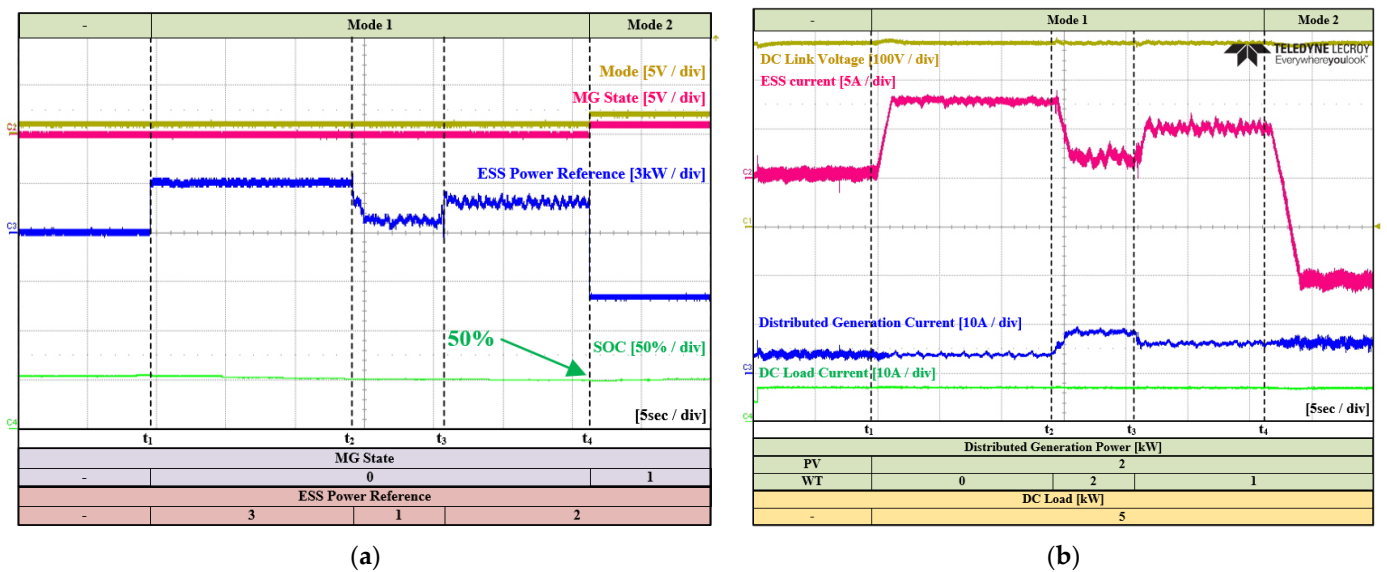

(a)

(b)

Figure 21. Experimental waveforms of microgrid operation Modes 1 and 2 in grid-connected operation (2): (**a**) waveforms of the input data (MG_{STATE}, SOC) and output data (Mode, ESS power reference) of ANN; (**b**) waveforms of the current of DG, DC load, and DC link voltage.

Figure 21a depicts the waveforms of the ANN as the inputs of MG_{STATE} and SOC, and *Mode* and *ESS Power Reference* are the outputs. The DC voltage of the microgrid, current of the DG converter, DC load, and the ESS current were as shown in Figure 21b. Table 3 lists the flow of each converter power in Modes 1 and 2 and in the forced charging mode.

Table 3. Microgrid power flow (2) in grid-connected operation.

Parameter	Value				Unit
	t_1–t_2	t_2–t_3	t_3–t_4	After t_4	
Mode	1	1	1	2	-
ESS	3	1	2	2	kW
PV	2	2	2	2	kW
WT	0	2	1	1	kW
ILC	0	0	0	5	kW
DC Load	5	5	5	5	kW

At t_1, the ANN was input, and the situation was given by Equation (1). The SOC decreased to less than 50% at t_4, and the ESS was forcibly charged by the ANN to prepare for the switch to the independent operation mode.

Figure 22 illustrates the experimental waveform for the ESS mode changing from the forced charge to the general charge/discharge operation when the SOC becomes 80%. Figure 22a illustrates the waveforms of the ANN as the output of MG_{STATE} and SOC, and *Mode* and *ESS Power Reference* are the inputs. The DC voltage of the microgrid, current of the DG converter, DC load, and the ESS current were as shown in Figure 22b. Table 4 lists the flow of each converter power in Modes 1 and 2 and in the forced charging mode.
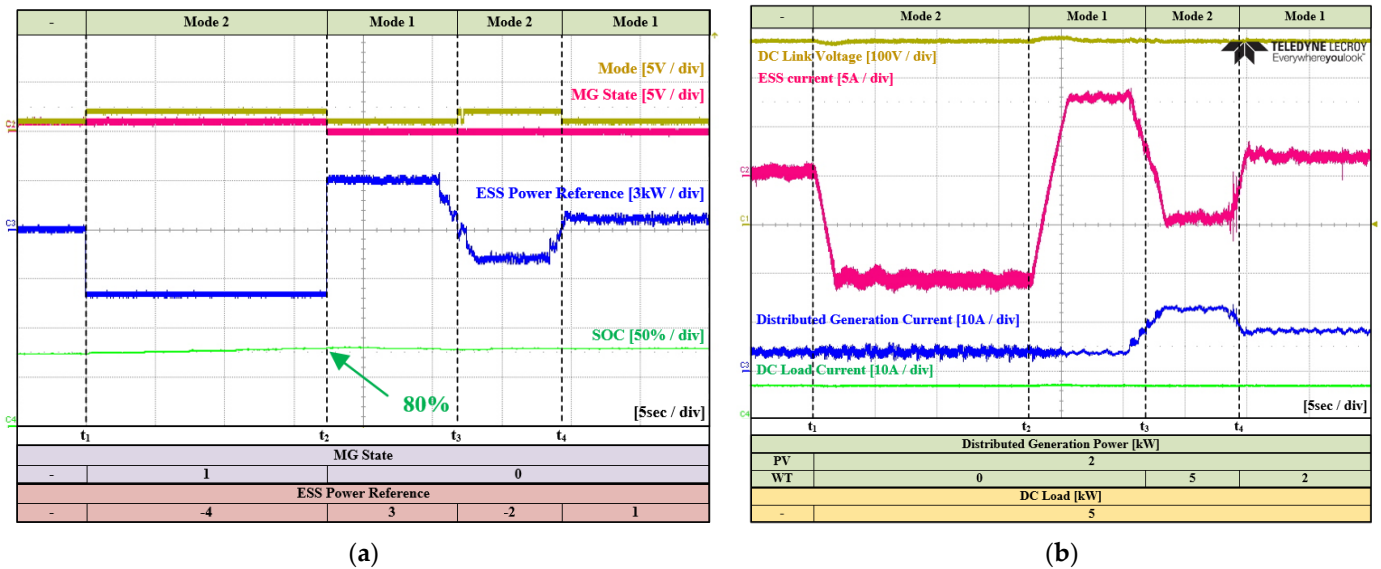

(a)　　　　　　　　　　　　　　　　　(b)

Figure 22. Experimental waveforms of microgrid operation Modes 1 and 2 in grid-connected operation (2): (**a**) waveforms of input data (MG_{STATE}, SOC) and output data (Mode, ESS power reference) of ANN; (**b**) waveforms of DC link voltage, current of ESS, DG, and DC load.

**Table 4.** Microgrid power flow (3) in grid-connected operation.

Parameter	Value				Unit
	t_1–t_2	t_2–t_3	t_3–t_4	After t_4	
Mode	2	1	2	1	-
ESS	−4	3	−2	1	kW
PV	2	2	2	2	kW
WT	0	0	5	2	kW
ILC	5	0	0	0	kW
DC Load	5	5	5	5	kW

At t_1, the ANN was the input, and during the period t_1–t_2, the ESS received power from the AC grid. At time t_2, the SOC of the ESS became 80%, and MG_{STATE} became zero; the ESS stopped forced charging according to the ANN's command, and it then performed normal charging and discharging operations.

3.2. Experimental Results in Standalone Operation

To simulate the standalone operation experiment, the main AC circuit breaker in Figure 2 was switched off to dispatch the AC grid. In standalone operation, the WT converter maintained DC voltage control, and the ILC performed AC voltage control.
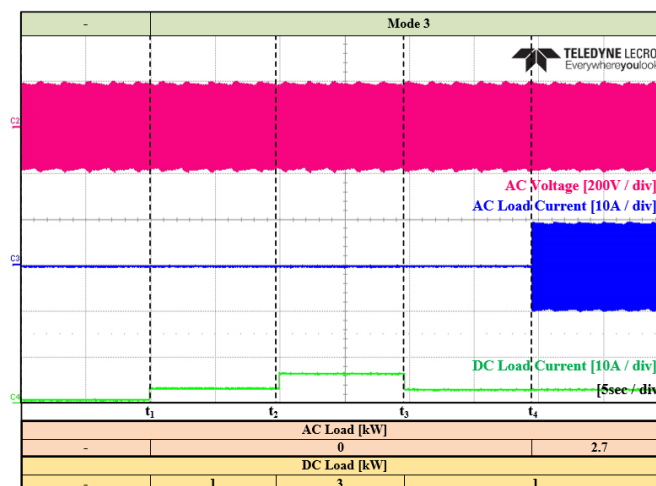
Figure 23 illustrates the experimental waveforms of Mode 3. In Mode 3, the ESS conducted charging and discharging depending on the command of the ANN when the SOC was between 20 and 90%.
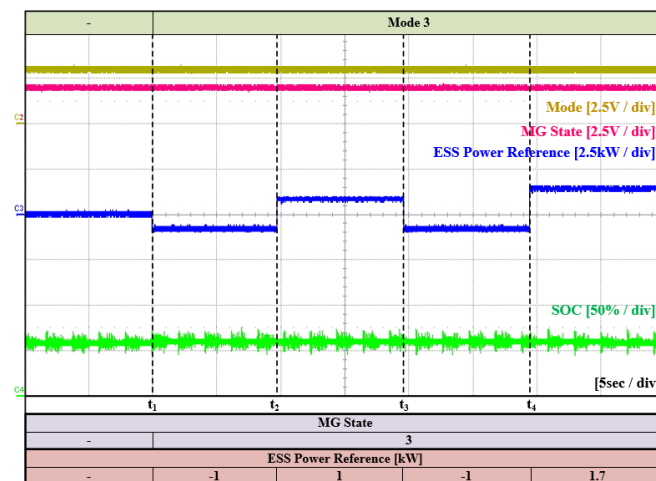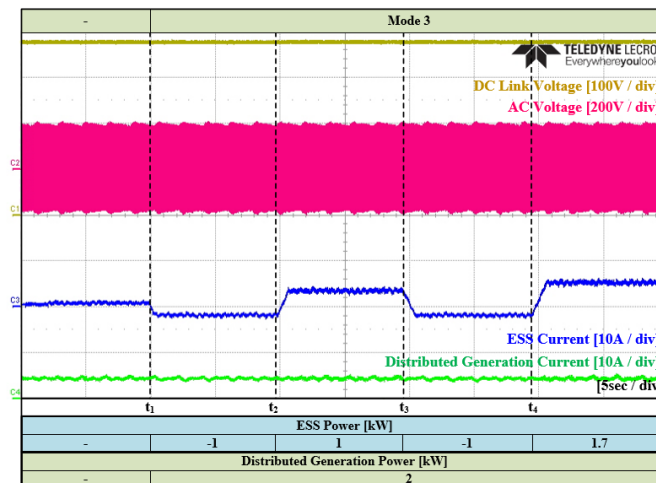
Figure 23. Experimental waveforms of standalone Mode 3. (**a**). Waveforms of the input data (MG state, SOC) and output data (Mode, ESS power reference) of the ANN. (**b**) Waveforms of DC link and AC voltage, ESS, and DG current. (**c**) Waveforms of each load current and AC grid voltage.

Figure 23a shows the waveforms of ANN as the output of MG_{STATE}, and SOC, Mode, and ESS Power Reference are the inputs. Figure 23b illustrates the voltages of the AC and

DC grids as well as the DGs' and ESS's current waveforms. Figure 23c shows the AC grid voltage and AC and DC load currents. Table 5 lists the flow of each converter's power in Mode 3.

Table 5. Microgrid power flow (1) during standalone operation.

Parameter	Value				Unit
	t_1–t_2	t_2–t_3	t_3–t_4	After t_4	
Mode	3	3	3	3	-
ESS	−1	1	−1	1.7	kW
PV	2	2	2	2	kW
WT		DC Voltage Control			kW
ILC	0	0	0	−2.7	kW
DC Load	1	3	1	1	kW
AC Load	0	0	0	2.7	kW

The ANN was input at time t_1; the situations in sections t_1–t_2 and t_3–t_4 are expressed in Equation (2); section t_2–t_3 and those after t_4 are expressed in Equation (1), and ESS operation was determined by the output of the ANN.

Figure 24 illustrates the experimental waveform for Mode 4. When the SOC was over 90%, the voltage increased within the microgrid, and overcharging the ESS was of concern; therefore, the power generated by the DGs power was limited up to the load power, and the ESS did not charge. Figure 24a illustrates the MG State and SOC, which are the inputs of the ANN, and the Mode and ESS Power Reference, which are the outputs. Table 6 lists the flow of each converter power in Modes 3 and 4.
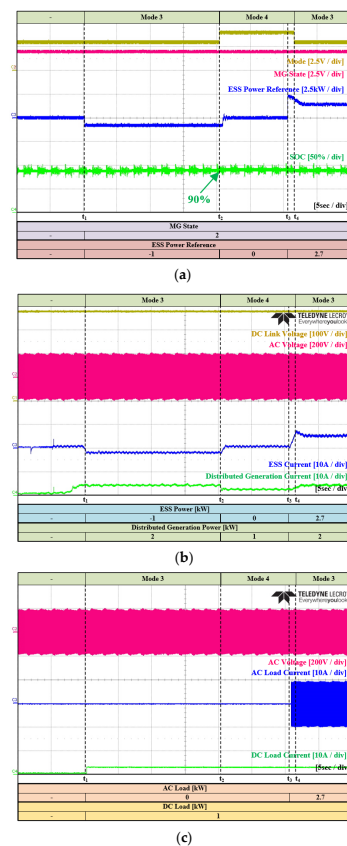

(a)

(b)

(c)

Figure 24. Experimental waveforms of standalone Modes 3 and 4. (**a**) Waveforms of the input data (MG state, SOC) and output data (Mode, ESS power reference) of the ANN. (**b**) Waveforms of DC link and AC voltage, ESS, and DG current. (**c**) Waveforms of each load current and AC grid voltage.

Table 6. Microgrid power flow (2) during standalone operation.

Parameter	Value				Unit
	t_1-t_2	t_2-t_3	t_3-t_4	After t_4	
Mode	3	4	4	3	-
ESS	−1	0	2.7	2.7	kW
PV	2	1	2	2	kW
WT		DC Voltage Control			kW
ILC	0	0	0	−2.7	kW
DC Load	1	1	1	1	kW
AC Load	0	0	0	2.7	kW

The ANN was input at time t_1, and it operated in Mode 3 in the period from t_1 to t_2. The generated power was greater than the load power; thus, the ESS performs its charging operation. The PV converter restricted the output power up to the load power, and the ESS stopped charging. Mode 4 was maintained for the period from t_2 to t_3. At time t_3, the load power became greater than the PV maximum power generation; therefore, the PV converter restricted the output power to 2 kW, and the ESS performed a discharge operation. In the subsequent section, the SOC was under 90%, and it was switched to Mode 3. Figure 24b,c illustrates the microgrid voltage, DG, and load current.

Figure 25 illustrates the experimental waveform of Mode 5, in which the SOC of the ESS fell below 20% during standalone operation, and the voltage drop of the distribution network and the overdischarge of the ESS were considered; thus, the load was cut off, and the ESS performs its charging operation. Figure 25a shows the MG State and SOC, which are the inputs of the ANN, and the *Mode* and *ESS Power Reference*, which are the outputs. Table 7 lists the changes in the power flow for each converter.

Table 7. Microgrid power flow (3) in standalone.

Parameter	Value		Unit
	t_1-t_2	After t_2	
Mode	3	5	-
ESS	1.7	−1	kW
PV	2	2	kW
WT	DC Voltage Control		kW
ILC	−2.7	0	kW
DC (Load)	1	1	kW
AC (Load)	2.7	0	kW

At time t_1, the ANN was input, and in the period t_1 to t_2, it operated in Mode 3. At time t_2, the SOC of the ESS became 20% and was switched to Mode 5. In this mode, the load, except for the critical DC loads, was forcibly cut off, and the ESS prioritized charging until the SOC reached 50%. Figure 25b,c illustrates the microgrid voltage, DG, and load current.

Figure 26 illustrates that when operating in Mode 5, the load was cut off until the SOC was over 50%, and the ESS charging operation was preferentially performed. When the SOC reached 50%, the operation mode switched to Mode 3, the load was connected again, and the ESS illustrated the experimental waveform performing the charge/discharge operation. Figure 26a shows the MG State and SOC, which are the inputs of the ANN, and the *Mode* and *ESS Power Reference*, which are the outputs. Table 8 lists the changes in the power flow for each converter.
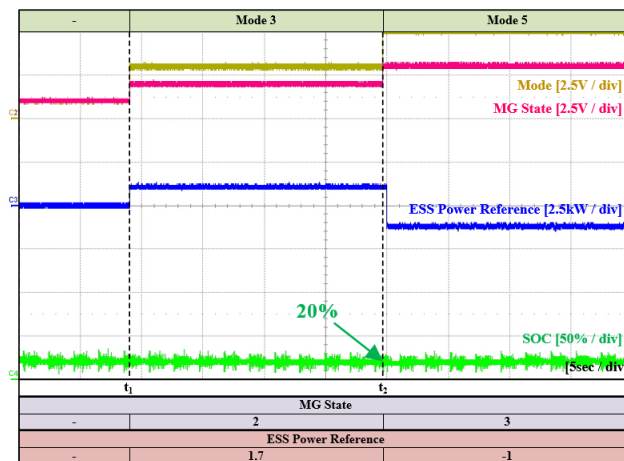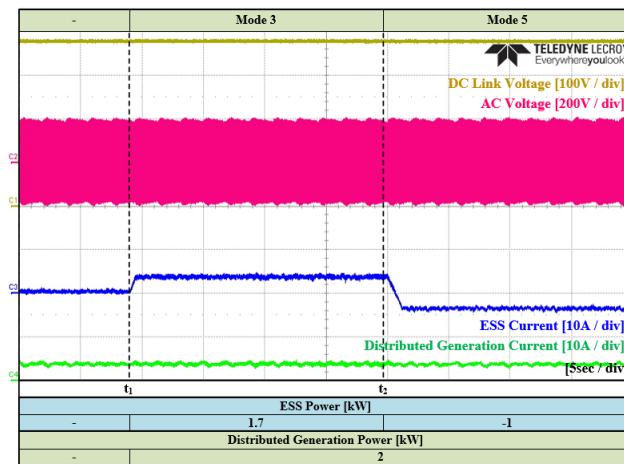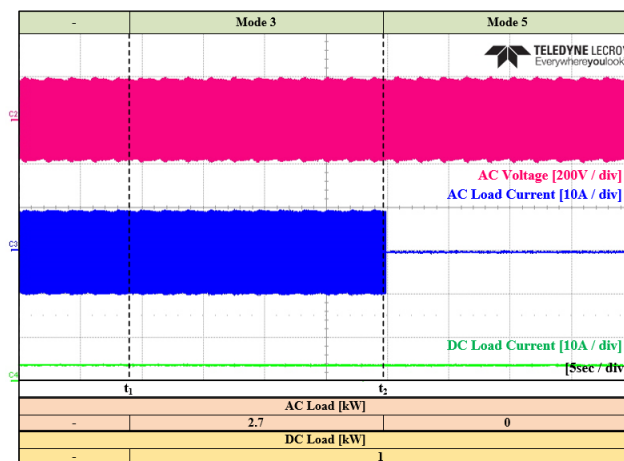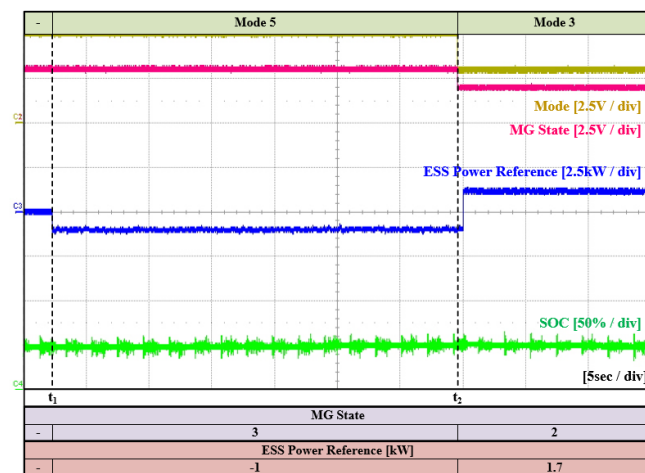
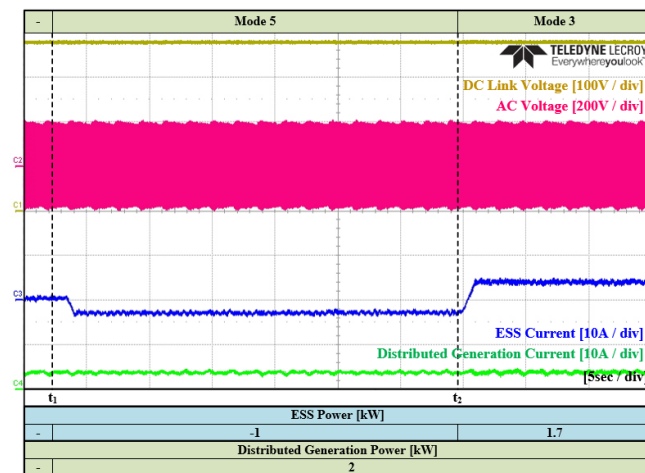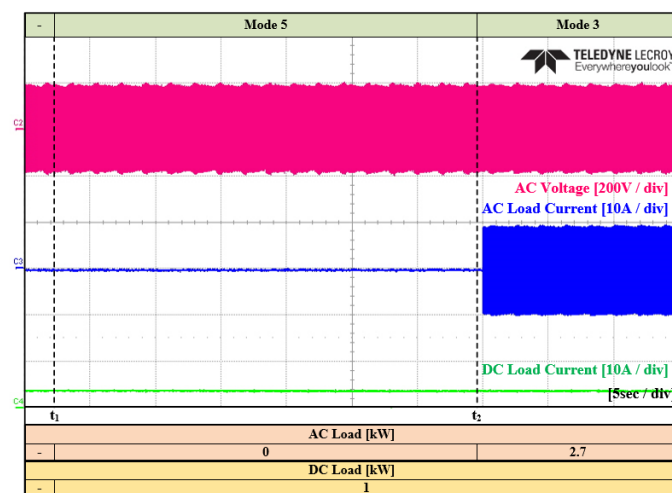**Figure 25.** Experimental waveforms of standalone Modes 3 and 5. (**a**). Waveforms of the input data (MG state, SOC) and output data (Mode, ESS power reference) of the ANN. (**b**) Waveforms of DC link and AC voltage, ESS, and DG current. (**c**) Waveforms of each load current and AC grid voltage.

(**a**)

(**b**)

(**c**)

Figure 26. Experimental waveforms of standalone Modes 5 and 3. (**a**) Waveforms of the input data (MG state, SOC) and output data (Mode, ESS power reference) of the ANN. (**b**) Waveforms of DC link and AC voltage, ESS, and DG current. (**c**) Waveforms of each load current and AC grid voltage.

Table 8. Microgrid power flow (2).

Parameter	Value		Unit
	t_1–t_2	After t_2	
Mode	5	3	-
ESS	−1	1.7	kW
PV	2	2	kW
WT	DC Voltage Control		kW
ILC	0	−2.7	kW
DC Load	1	1	kW
AC Load	0	2.7	kW

At time t_1, the artificial neural network was input, and in the period from t_1 to t_2, it operated in Mode 5. At time t_2, the SOC of the ESS became 50% and was switched to Mode 3. In this mode, all loads were reconnected, and the ESS performed its charging and discharging operations. Figure 26b,c illustrates the microgrid voltage, DG, and load current.

4. Conclusions

In this paper, a hybrid microgrid EMS was proposed. A hybrid microgrid has several typical difficulties in implementation because various power conversion devices and loads are connected. First, because many power conversion devices are linked through communication, a communication cycle with the MGCC becomes longer if there is a lot of transmission data. In addition, because the MGCC controls the operation of the entire converter, it is difficult to change the algorithm because it is complicated, and the ANN-based EMS has difficulty learning according to environmental changes. To address these implementation difficulties, in this study, a two-step ANN was applied to hybrid microgrid operation.

The microgrid applied in this paper consists of ILC, WT, PV, and ESS, and it has the form of a conventional hybrid microgrid. The microgrid has a master–slave control structure, and a two-step ANN was applied to the master, the MGCC. The first step of the ANN's process determines the operating mode of the microgrid with three inputs: microgrid state, net power, and SOC. The determined mode selects the control method of each individual converter. The second step of the ANN's process determines the ESS power command with three inputs: operation mode, net power, and SOC. The ESS is controlled by the determined ESS power reference. The two-step ANN mentioned above shows that microgrid operation is possible even though communication data is minimal. In addition, because two ANNs are serially configured, only a single ANN can be changed, making it easy to apply to a new environment. Because the two-step ANN has a simple structure and shows high accuracy even with a small number of repeated learning epochs, it is easier to learn and apply the ANN to the field than a conventional EMS.

In conclusion, the proposed microgrid operation method applies an ANN to the operation method to use distributed power generation and load demand power data on a small-scale microgrid. In the experimental process, it was confirmed that the operating mode, which is the result of first step, and the power command of the ESS, which is the result of the second step, stably operated under variable loads and DGs conditions, and the individual converters were controlled by the MGCC.

Through this experiment, the feasibility of operating a small-scale microgrid by an ANN was verified, and the validity of this study was proved. In the future, many studies and ideas related to hybrid AC/DC microgrid EMSs and nonlinear load problems using ANNs are expected.

References

1. Li, X.; Song, Y.J.; Han, S.B. Study on Power Quality Control in Multiple Renewable Energy Hybrid Micro Grid System. In Proceedings of the 2007 IEEE Lausanne Power Tech, Lausanne, Switzerland, 1–5 July 2007; pp. 2000–2005.
2. Prabhala VA, K.; Baddipadiga, B.P.; Ferdowsi, M. DC distribution systems-An overview. In Proceedings of the 2014 International Conference on Renewable Energy Research and Application (ICRERA), Milwaukee, WI, USA, 19–22 October 2014; pp. 307–312.
3. Abbasi, M.; Abbasi, E.; Li, L.; Aguilera, R.P.; Lu, D.; Wang, F. Review on the Microgrid Concept, Structures, Components, Communication Systems, and Control Methods. *Energies* **2023**, *16*, 484. [CrossRef]
4. Navas-Fonseca, A.; Burgos-Mellado, C.; Gomez, J.S.; Donoso, F.; Tarisciotti, L.; Saez, D.; Cardenas, R.; Sumner, M. Distributed Predictive Secondary Control for Imbalance Sharing in AC Microgrids. *IEEE Trans. Smart Grid* **2021**, *13*, 20–37. [CrossRef]
5. Dragicevic, T.; Lu, X.; Vasquez, J.C.; Guerrero, J.M. DC microgrids—Part II: A review of power architectures, applications, and standardization issues. *IEEE Trans. Power Electron.* **2015**, *31*, 3528–3549. [CrossRef]
6. Ali, S.; Zheng, Z.; Aillerie, M.; Sawicki, J.-P.; Péra, M.-C.; Hissel, D. A Review of DC Microgrid Energy Management Systems Dedicated to Residential Applications. *Energies* **2021**, *14*, 4308. [CrossRef]
7. Nejabatkhah, F.; Li, Y.W. Overview of Power Management Strategies of Hybrid AC/DC Microgrid. *IEEE Trans. Power Electron.* **2014**, *30*, 7072–7089. [CrossRef]
8. Espina, E.; Llanos, J.; Burgos-Mellado, C.; Cardenas-Dobson, R.; Martinez-Gomez, M.; Saez, D. Distributed Control Strategies for Microgrids: An Overview. *IEEE Access* **2020**, *8*, 193412–193448. [CrossRef]
9. Gao, F.; Wang, X.; Yang, P.; Kou, S.; Sun, M. Research and Simulation of Hybrid AC/DC Microgrid. In Proceedings of the 2020 4th International Conference on HVDC (HVDC), Xi'an, China, 6–9 November 2020; pp. 1276–1280. [CrossRef]
10. Wang, L.; Fu, X.; Wong, M.-C.W. Operation and Control of a Hybrid Coupled Interlinking Converter for Hybrid AC/Low Voltage DC Microgrids. *IEEE Trans. Ind. Electron.* **2020**, *68*, 7104–7114. [CrossRef]
11. Li, X.; Guo, L.; Li, Y.; Guo, Z.; Hong, C.; Zhang, Y.; Wang, C. A Unified Control for the DC–AC Interlinking Converters in Hybrid AC/DC Microgrids. *IEEE Trans. Smart Grid* **2017**, *9*, 6540–6553. [CrossRef]
12. An, C.-G.; Choi, B.-Y.; Lee, H.; Kim, T.-G.; Kang, K.-M.; Kim, M.; Lee, Y.-S.; Yi, J.; Won, C.-Y. Space Vector Pulse-Width Modulation Control Strategy for Four-Leg Inverters Under Single Line-to-Ground Faults in Islanded Microgrids. *IEEE Access* **2022**, *10*, 18557–18569. [CrossRef]
13. Morstyn, T.; Hredzak, B.; Agelidis, V.G. Control Strategies for Microgrids with Distributed Energy Storage Systems: An Overview. *IEEE Trans. Smart Grid* **2016**, *9*, 3652–3666. [CrossRef]
14. Bani-Ahmed, A.; Rashidi, M.; Nasiri, A.; Hosseini, H. Reliability Analysis of a Decentralized Microgrid Control Architecture. *IEEE Trans. Smart Grid* **2018**, *10*, 3910–3918. [CrossRef]
15. Papadaskalopoulos, D.; Pudjianto, D.; Strbac, G. Decentralized Coordination of Microgrids with Flexible Demand and Energy Storage. *IEEE Trans. Sustain. Energy* **2014**, *5*, 1406–1414. [CrossRef]
16. Gavriluta, C.; Candela, J.I.; Citro, C.; Rocabert, J.; Rodriguez, P. Decentralized Primary Control of MTDC Networks with Energy Storage and Distributed Generation. *IEEE Trans. Ind. Appl.* **2014**, *50*, 4122–4131. [CrossRef]
17. Kermani, M.; Carnì, D.L.; Rotondo, S.; Paolillo, A.; Manzo, F.; Martirano, L. A Nearly Zero-Energy Microgrid Testbed Laboratory: Centralized Control Strategy Based on SCADA System. *Energies* **2020**, *13*, 2106. [CrossRef]
18. Han, Y.; Ning, X.; Yang, P.; Xu, L. Review of power sharing, voltage restoration and stabilization techniques in hierarchical controlled DC microgrids. *IEEE Access* **2019**, *7*, 149202–149223. [CrossRef]
19. Che, L.; Shahidehpour, M.; Alabdulwahab, A.; Al-Turki, Y. Hierarchical Coordination of a Community Microgrid with AC and DC Microgrids. *IEEE Trans. Smart Grid* **2015**, *6*, 3042–3051. [CrossRef]
20. Salomonsson, D.; Soder, L.; Sannino, A. An Adaptive Control System for a DC Microgrid for Data Centers. *IEEE Trans. Ind. Appl.* **2008**, *44*, 1910–1917. [CrossRef]

21. Kang, K.-M.; Choi, B.-Y.; Lee, H.; An, C.-G.; Kim, T.-G.; Lee, Y.-S.; Kim, M.; Yi, J.; Won, C.-Y. Energy Management Method of Hybrid AC/DC Microgrid Using Artificial Neural Network. *Electronics* **2021**, *10*, 1939. [CrossRef]

22. Kotra, S.; Mishra, M.K. Energy management of hybrid microgrid with hybrid energy storage system. In Proceedings of the 2015 International Conference on Renewable Energy Research and Applications (ICRERA), Palermo, Italy, 22–25 November 2015; pp. 856–860. [CrossRef]

23. Bhavsar, Y.S.; Joshi, P.V.; Akolkar, S.M. Simulation of Microgrid with energy management system. In Proceedings of the 2015 International Conference on Energy Systems and Applications, Pune, India, 30 October–1 November 2015; pp. 592–596. [CrossRef]

24. Tank, I.; Mali, S. Renewable based DC microgrid with energy management system. In Proceedings of the 2015 IEEE International Conference on Signal Processing, Informatics, Communication and Energy Systems (SPICES), Kozhikode, India, 19–21 February 2015; pp. 1–5. [CrossRef]

25. Yu, L.; Qin, S.; Zhang, M.; Shen, C.; Jiang, T.; Guan, X. A Review of Deep Reinforcement Learning for Smart Building Energy Management. *IEEE Internet Things J.* **2021**, *8*, 12046–12063. [CrossRef]

26. Kim, W.J.; Kim, S.H. Multiple Switches Open-Fault Diagnosis Using ANNs of Two-Step Structure for Three-Phase PWM Converters. In *Proceedings of the KIPE Conference*; The Korean Institute of Power Electronics: Jeju, Republic of Korea, 2020; pp. 282–283.

27. Mohd, A.; Ortjohann, E.; Hamsic, N.; Sinsukthavorn, W.; Lingemann, M.; Schmelter, A.; Morton, D. Control strategy and space vector modulation for three-leg four-wire voltage source inverters under unbalanced load conditions. *IET Power Electron.* **2010**, *3*, 323–333. [CrossRef]